CrossMark

ARTICLE

Edge-Dependent Electronic and Magnetic Characteristics of Freestanding β_{12}-Borophene Nanoribbons

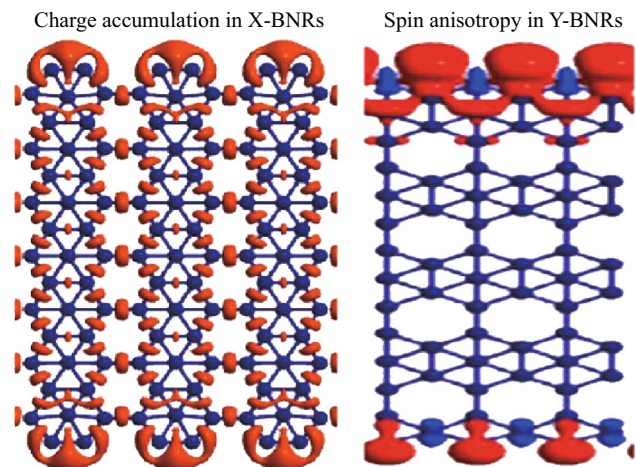Sahar Izadi Vishkayi[1] · Meysam Bagheri Tagani[1]

Highlights

- Nanoribbons produced by cutting a β_{12} borophene sheet (BNR) were studied using ab-initio calculations.
- Charge accumulation was observed at the edge of X-BNRs, which make them good candidates for gas sensors.
- Y-BNRs are potential candidates for spintronics due to strong spin anisotropy.

Abstract This work presents an investigation of nanoribbons cut from β_{12}-borophene sheets by applying the density functional theory. In particular, the electronic and magnetic properties of borophene nanoribbons (BNR) are studied. It is found that all the ribbons considered in this work behave as metals, which is in good agreement with the recent experimental results. β_{12}-BNR has significant diversity due to the existence of five boron atoms in a unit cell of the sheet. The magnetic properties of the ribbons are strongly dependent on the cutting direction and edge profile. It is interesting that a ribbon with a specific width can behave as a normal or a ferromagnetic metal with magnetization at just one edge or two edges. Spin anisotropy is observed in some ribbons, and the magnetic moment is not found to be the same in both edges in an antiferromagnetic configuration. This effect stems from the edge asymmetry of the ribbons and results in the breaking of spin degeneracy in the band structure. Our

Charge accumulation in X-BNRs   Spin anisotropy in Y-BNRs

findings show that β_{12} BNRs are potential candidates for next-generation spintronic devices.

✉ Meysam Bagheri Tagani
m_bagheri@guilan.ac.ir

[1] Department of Physics, Computational Nanophysics Laboratory (CNL), University of Guilan, Po Box: 41335-1914, Rasht, Iran

🖄 Springer

1 Introduction

Borophene, a single layer of boron atoms, has been recently synthesized in an ultra-high vacuum condition by two independent groups [1, 2]. The initial reports had some differences. The borophene synthesized by Mannix et al. [1] was buckled, whereas Feng et al. [2] presented two flat phases as β_{12} and χ_3 [3]. Later, it was demonstrated that the buckling observed in Ref. [1] can be attributed to the undulation of the first layer of the substrate [4], and the synthesized borophene phase is β_{12}. The next analysis showed that the β_{12} borophene is a metal [5], and the structure can host the Dirac cone [6, 7].

After these two successful experimental syntheses of borophene sheets, a lot of theoretical research has been devoted to the study of borophene properties in recent years [8–18]. The mechanical properties of several borophene sheets have been investigated, and their ideal strength, ultimate strain, and Young's modulus have been reported [16, 18–22]. Superconductivity [23–27] and thermal conductivity [13, 28] of borophene sheets have also been studied. It was predicted that their superconductivity could be modulated by the strain, while their thermal conductivity is low. Furthermore, oxidized [11, 29] and hydride [30–32] borophene sheets have been examined, and it was found that the oxygen or hydrogen absorption reduces the anisotropy of the structure. Borophene sheets can also be considered as good anodes for Li- and Na-ion storage [33–35]. It has been shown that the structural anisotropy of the borophene can lead to the direction-dependent current–voltage characteristics [36, 37].

Cutting two-dimensional (2D) structures along one direction makes them as one-dimensional nanoribbons. Nanoribbons have electronic, magnetic, and optical properties, which are different from 2D structures. It is well known that the zigzag-edge graphene nanoribbons are metals, while the armchair-edge nanoribbons are either metals or semiconductors—with respect to the ribbon width [38, 39]. Garcia-Fuente et al. [9] studied borophene nanoribbons (BNRs) produced from *2Pmmn* and *8Pmmn* borophene sheets. They found that *8Pmmn* BNRs are more stable and have properties that are more interesting. Nanoribbons can be nonmagnetic or magnetic depending on the cutting directions. In addition, the *8Pmmn* BNRs can be a metal or semiconductor with respect to the cutting direction and their width. Meng et al. [40] investigated *2Pmmn* BNRs and reported that the ribbons produced by cutting the sheet along *x*-direction are metal, whereas the ribbons produced from cutting in *y*-direction can be magnetic. They also found that upon hydrogenation all nanoribbons become nonmagnetic.

Zhong et al. [41] have reported successful synthesis of BNRs on Ag (110) surfaces very recently. They also observed several phases of BNRs, such as χ_3, β, and β_8. These experimental works have provided motivation for us to study the electronic and magnetic properties of β_{12} BNRs using the density functional theory for the first time. The results show that all the BNRs considered in our work are metals, and the edge magnetization is dependent on the cutting direction. In addition, we observed that some ribbons are magnetic at just one edge. It is also observed that the spin anisotropy of the edge states is attributed to the reconstruction of the edge. The electron density analysis reveals that a charge accumulation occurs in some edges, which is consistent with the recent experimental results [42].

The next section discusses the simulation methods. The simulation results are presented in Sect. 3. We analyze the binding energy, electron density, transmission channel, electron localized function, band structure, and magnetization of the considered ribbons in detail.

2 Simulation Details

All calculations are performed using the density functional theory (DFT) implemented in the SIESTA package [43]. The interaction between the valance and core electrons is described by norm-conserved Troullier–Martins pseudopotentials [44]. Perdew–Burke–Ernzerhof (PBE) [45] generalized gradient approximation (GGA) is employed as the exchange–correlation functional. The cutoff energy is *200 Ry*. The Brillouin zone of the β_{12} borophene sheet is sampled using a $31 \times 41 \times 1$ Monkhorst *k*-point mesh size, and 100 *k*-points centered at the Γ-point are used in direction where the ribbon is periodic. We considered a 30 Å vacuum to eliminate the interlayer interactions in nonperiodic directions of the ribbons. All ribbons are fully relaxed until the force converges to 0.001 eV Å^{-1}. To investigate the magnetic properties of the ribbons, a supercell comprising two unit cells is employed in the optimization process. Thirteen orbitals are employed for each boron atom, consisting of two sets of orbitals of the *s* type, two sets of *p* type, and one set of *d* type, with cutoff radii of 2.8, 3.35, and 3.35 Å, respectively.

3 Results and Discussion

Figure 1 shows an optimized β_{12}-borophene sheet with five boron atoms in the unit cell. Lattice constants of the sheet are equal to $a = 5.15$ Å and $b = 2.97$ Å, which are in good agreement with previous works [2, 3, 5]. The sheet has uniform vacancies that compensate the electron
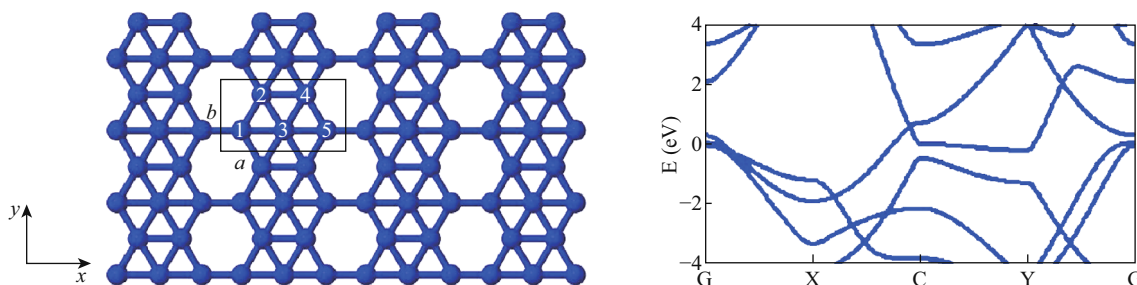
Fig. 1 Scheme of the freestanding β_{12}-borophene sheet. The unit cell is shown by the rectangle with a and b vectors (left panel). The band structure of the freestanding β_{12}-borophene sheet (right panel)

deficiency of the boron atoms and stabilize the structure. The band structure of the freestanding borophene sheet indicates that the structure is metal, like other reported borophene sheets [1, 2, 8, 14, 37]. Cutting the borophene along the x- or y-direction gives rise to the formation of nanoribbons with different edge shapes. The edge profile and the width of ribbons are key factors in the electronic and magnetic properties of the ribbons. Therefore, one can expect that the cutting direction is very important. In this research, we focus on two cutting directions: along x or y.

The BNRs provided by the cutting of the sheet along the x-direction are denoted by *NuvXBNR*, where N is the number of boron atoms in a row of the ribbon unit cell, and $u(v)$ stands for the edge shape of a ribbon unit cell, which can be composed of two boron atoms (hereafter denoted by A) or three boron atoms (hereafter denoted by B). It is
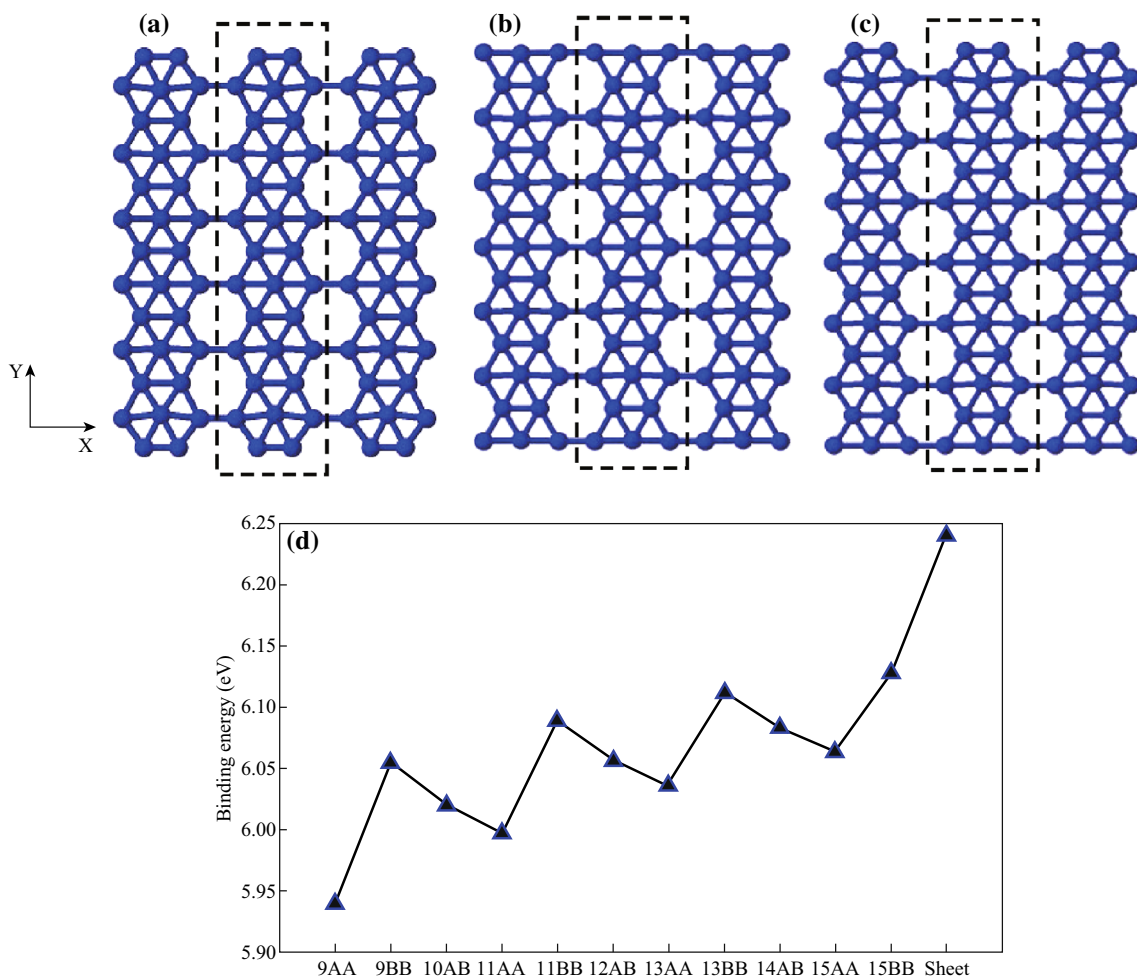

Fig. 2 Structure of **a** *13AAXBNR*, **b** *13BBXBNR*, and **c** *14ABXBNR*. **d** The binding energy of the considered structures. The dashed rectangle shows the unit cell of each ribbon

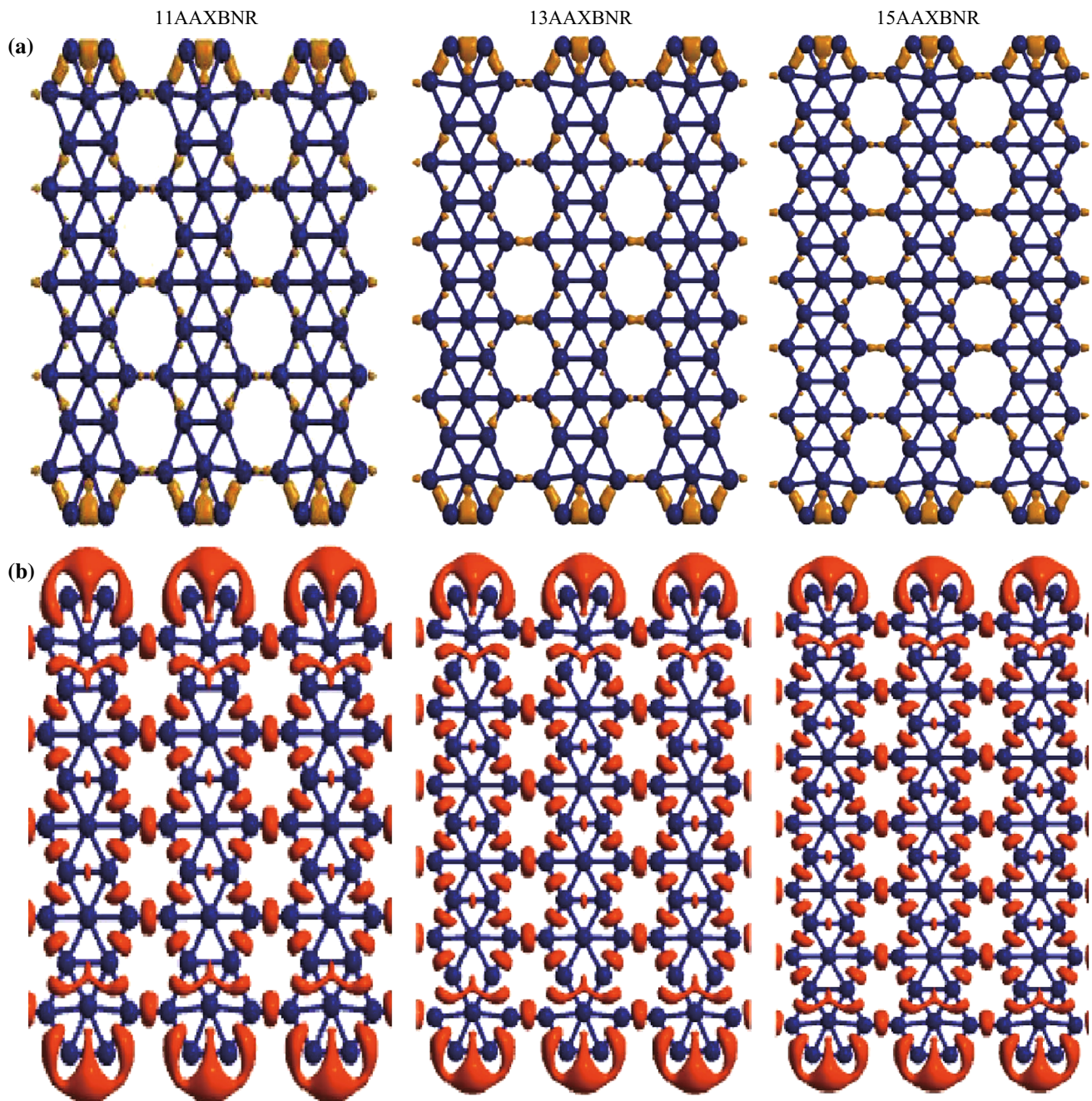11AAXBNR   13AAXBNR   15AAXBNR

Fig. 3 a The electron density and **b** the electron localized function (ELF) of *11AAXBNR*, *13AAXBNR*, and *15AAXBNR*

obvious from Fig. 1 that the ribbons with even *N* are *AB* and the ones with odd *N* are *AA* or *BB*. We consider the ribbons with widths in the range from $N = 9$ to $N = 15$ so that the maximum width of the ribbon is 21 Å. An analysis of the optimized *NuvXBNRs* shows that all the structures are normal metals, and no magnetization is seen at the edges. In addition, the ribbons are flat structures without buckling, compared to the β_{12}-borophene sheets. Figure 2a–c shows the structure of 13*AA*, 13*BB*, and 14*ABXBNR*, respectively.

For *NAAXBNRs*, the bonding lengths of the edge boron atoms are 0.2 Å shorter than the bonding length in the sheet. Furthermore, the angle of the bonding between three boron atoms next to the edge atoms is deviated from the line (180°) and is equal to 167°, leading to the deformation of the hexagonal ring near the edge of the ribbon. The binding energy, $E = -\frac{E_{NuvXBNR} - NE_B}{N}$, of the structures is plotted in Fig. 2e, where E_B stands for the energy of an isolated boron atom. It is observed that *NAAXBNRs* have the lowest energy so that their binding energy is even lower

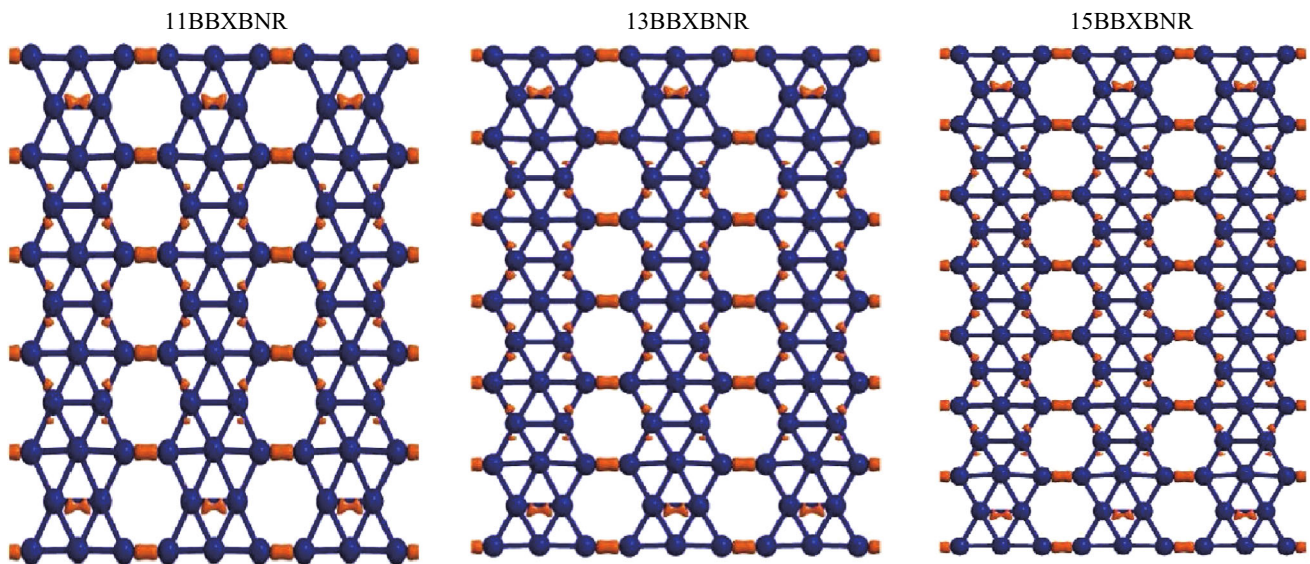11BBXBNR　　　　　　　　　13BBXBNR　　　　　　　　　15BBXBNR

Fig. 4 Electron density of *11BBXBNR*, *13BBXBNR*, and *15BBXBNR*

than $(N-1)ABXBNR$. The increment of the ribbon width gives rise to the increase in the binding energy. The electron density and the electron localized function (ELF) of the *NAAXBNRs* are shown in Fig. 3. Figure 3a indicates that the electron is accumulated at the edge of the ribbons, which is in agreement with recent experimental results. Scanning tunneling microscopy results of Refs. [41, 42] showed that the electrons are accumulated in the boundary of the β_{12} sheet. In addition, it has recently been reported that the edge of the β-borophene ribbons hosts more electrons than the body of the ribbon. The ELF also supports the above results so that the electrons are completely localized at the edge of the ribbons. The primary reason behind the observation arises from the low coordination of the edge atoms. Passivation of the edge atoms can eliminate the charge accumulation like what is observed in the graphene nanoribbons. Our findings show that the edge of the borophene ribbons is able to absorb atoms and molecules. Mannix et al. reported that their synthesized borophene was partially hydrogenated [1], which can be attributed to the edge absorption with respect to our results. In supplementary information, we examine the hydrogen absorption in a unit cell of *13AAXBNR* with two different scenarios: absorption in an edge or in the body. Interestingly, we observe that the body absorption destructs the ribbon, whereas the absorption at the edge removes electron accumulation and preserves its initial configuration, as shown in Figs. S9 and S10.

In our observation, *NBBXBNRs* are more stable than *NAAXBNRs*. The bonding length of the edge boron atoms is 3% shorter than the sheet. In addition, the bonding of the edge boron atoms with the boron atoms next to the edge is stronger in the ribbon due to the shorter bond length. The

electron density analysis results (Fig. 4) show that the electrons are accumulated in the body of the ribbon dissimilar to *NAAXBNR*. By comparison with Fig. 3a, one can claim that the ribbons with the *A* kind edge are more inclined to absorb atoms and molecules via the edge. Note that the A-type atoms have five bonds in the sheet but three in the ribbon. In contrast, the B-type toms make four bonds in the sheet and three bonds in the ribbon. As a result, electron localization is more in *NAAXBNRs* than in *NBBXBNRs*. The band structure and the transmission channel per spin of *NAAXBNRs* and *NBBXBNRs* are plotted in Fig. 5. It can be seen that all the structures are metals. The transmission channel was computed by counting of the energy bands crossing a specific energy. The transmission channel can be considered as the transmission coefficient in low temperatures and with perfect coupling. Figure 6 shows the electron density and the band structure of *NABXBNRs*, which are composed of *A*- and *B*-type edges. As mentioned above, the electron accumulation is observed in the *A*-type edge, similar to *NAAXBNR*. The *AB* edge ribbons are also metal, and their transmission channel increases by the increase in the ribbon width. Ab initio molecular dynamics (AIMD) simulation shows that the XBNRs are thermally stable at 500 K, as shown in Fig. S11.

The following section investigates the ribbons obtained by cutting the borophene sheet along the *y*-direction. As shown in Fig. 1, five boron atoms of a β_{12}-borophene unit cell have different *x* positions, numbered 1–5 in Fig. 1. As a result, there is a large set of variations in the ribbons. We name each ribbon as *NYuvBNR*, where u, $v = 1...5$. Here, u and v denote the number of the boron atoms that is in the bottom or top edge, respectively. *N* stands for the number
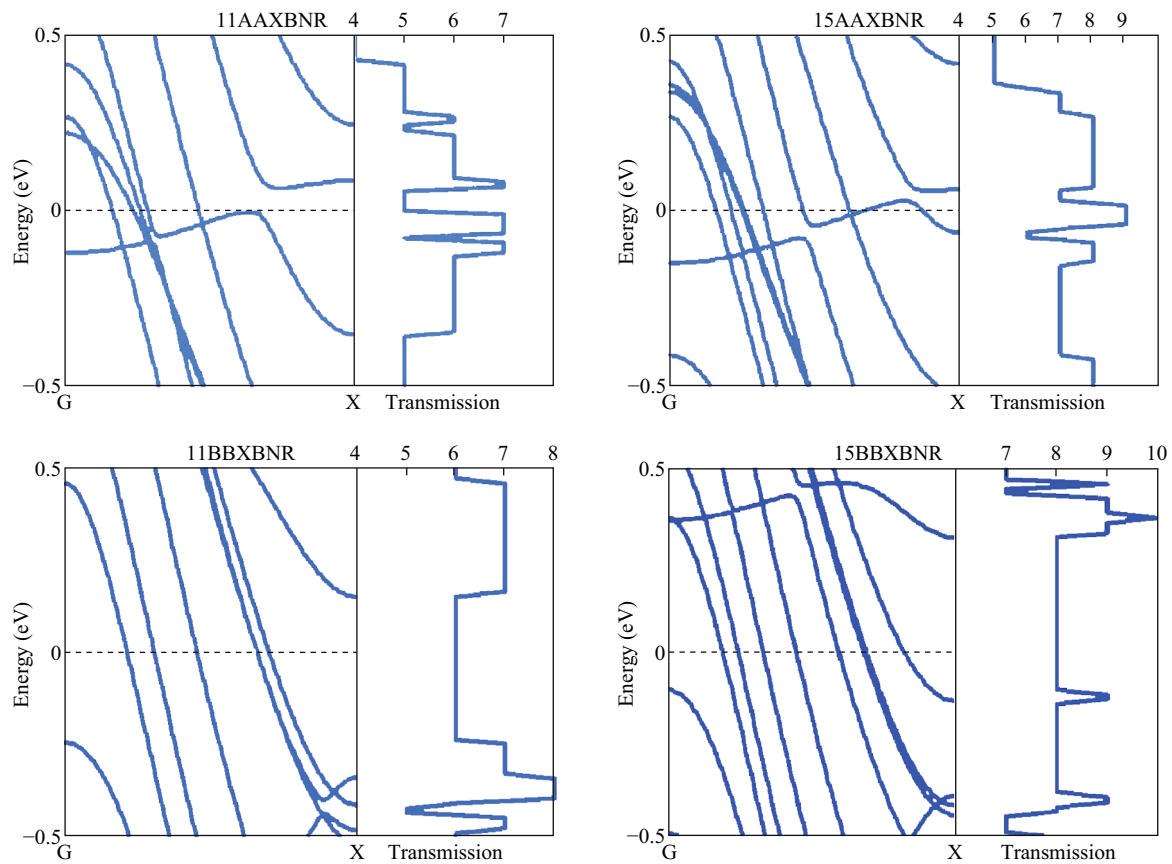
Fig. 5 Band structure and the transmission channel of *11AAXBNR*, *15AAXBNR*, *11BBXBNR*, and *15BBXBNR*

of boron atoms in a unit cell of the ribbon and describes the width of the ribbon. We investigate the ribbons with $N = 20$ to $N = 25$ so that the maximum width of the ribbon studied here is 24 Å. We found that for each N there are three different edge configurations. Therefore, 18 ribbons are studied in detail. It is interesting to note that there are just two distinct configurations for ribbons created from 2*Pmmn* and 8*Pmmn* borophene sheets [15], but here, we are faced with more diversity. This diversity leads to more complexity of the β_{12}-BNRs along y-direction.

The total energy per atoms of *NYBNRs* is plotted in Fig. 7. The total energy analysis shows that the *NYBNRs*, unlike *NXBNRs*, can be magnetic in some widths. First, we study the allotropes of 20*YBNR* and 25*YBNR*, which have the same configurations. The increase in the ribbon width strengthens the stability of the ribbons, which is clear with more energy of 25*YBNRs* than 20*YBNRs*. Although some allotropes are magnetic, the ground state, 20*Y32BNR* and 25*Y32BNR*, is nearly nonmagnetic. The optimized structures of 20*YBNRs* are plotted in Fig. S1. We find that the edge configuration, bonding length, and the existence of fully occupied hexagonal lattices or hexagonal hole lattices are key factors in determining electronic and magnetic properties of the ribbons. The electron localization function

of 20*YBNR* allotropes is plotted in Fig. 8a. It is clear that the edge significantly affects the localization of the electron. As shown in Fig. 8a, the electrons are localized in two edges of 20*Y15* and 20*Y12* leading to the magnetization of the structures. On the contrary, the electron density is distributed between two boron atoms at the edge of 20*Y32BNR*, especially at the edge with hexagonal holes. We found that the edges with hexagon holes are nonmagnetic, whereas ones with fully occupied hexagonal rings are magnetic. A minor electron localization is observed in the bottom edge of 20*Y32*. As a result, the energy of the magnetic state of 20*Y32* is a few *meV* more than the nonmagnetic one. The highest electron localization is observed in 20*Y21*. Therefore, the energy difference between its magnetic and nonmagnetic states is higher. We expect that if the ribbons grow on the substrate, the interaction between the boron atoms and the substrate becomes strong in some ribbons like 20*Y21*, and the electron transfer between the ribbon and the substrate reduces the magnetization. For the magnetic state, we considered both ferromagnetic (two edges with same majority spin orientation) and antiferromagnetic (two edges with opposite majority spin orientation) configurations and found that they are degenerate. The spin density of the allotropes of
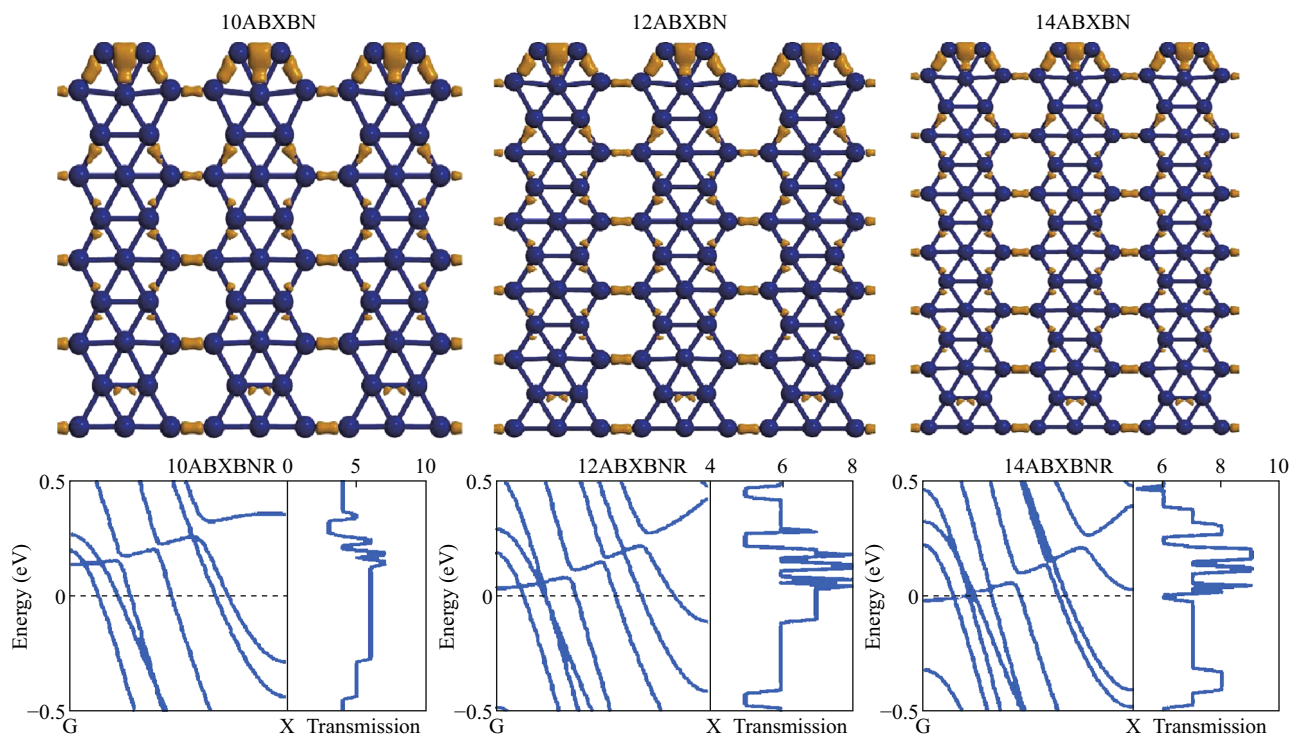
Fig. 6 Electron density (upper panels), the band structure, and the transmission channel (lower panels) of *10ABXBNR*, *12ABXBNR*, and *14ABXBNR*
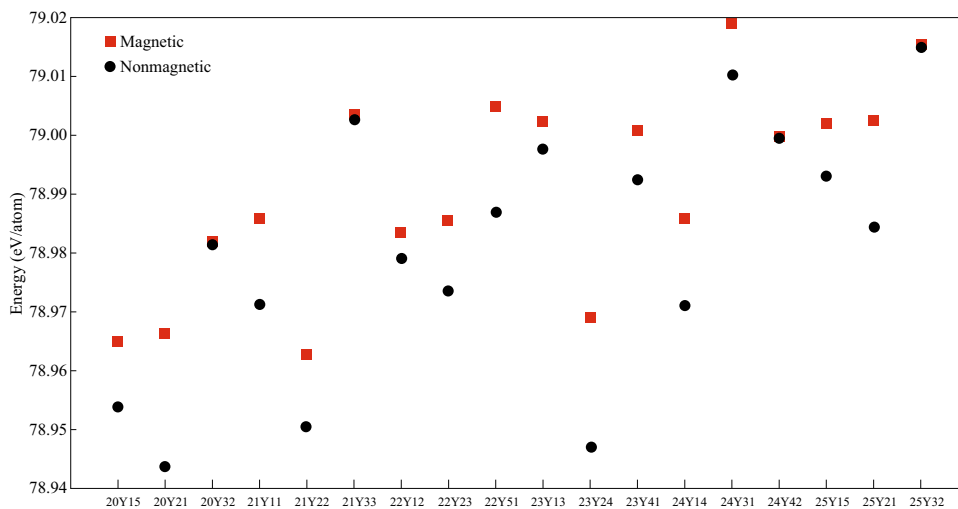

Fig. 7 Total energy per atom of *NYuvBNRs*

20YBNR is depicted in Fig. 8b in the ferromagnetic configuration. The maximum of magnetic moment is equal to 0.58 μ_B for *20Y15*, and to 0.7 μ_B for *20Y21*. A spin anisotropy is found in *20Y21* with a magnetic moment of 0.7 μ_B in the top edge and 0.68 μ_B in the bottom edge. The anisotropy is directly dependent on the structural anisotropy and the inequality of bond length in two edges of the ribbon. The spin anisotropy is amplified in other widths of

the *NYBNR*. The band structure of *20YBNRs* is plotted in Fig. S4, which shows all the ribbons to be metals.

The total energy analysis shows that the ribbons with $N = 22$, 23, and 24 are magnetic—independent of the edge profile. In the following section, we analyze the most stable configurations of the ribbons discussed thus far and investigate the origin of the edge magnetization. The remaining ribbons are discussed in Supplementary
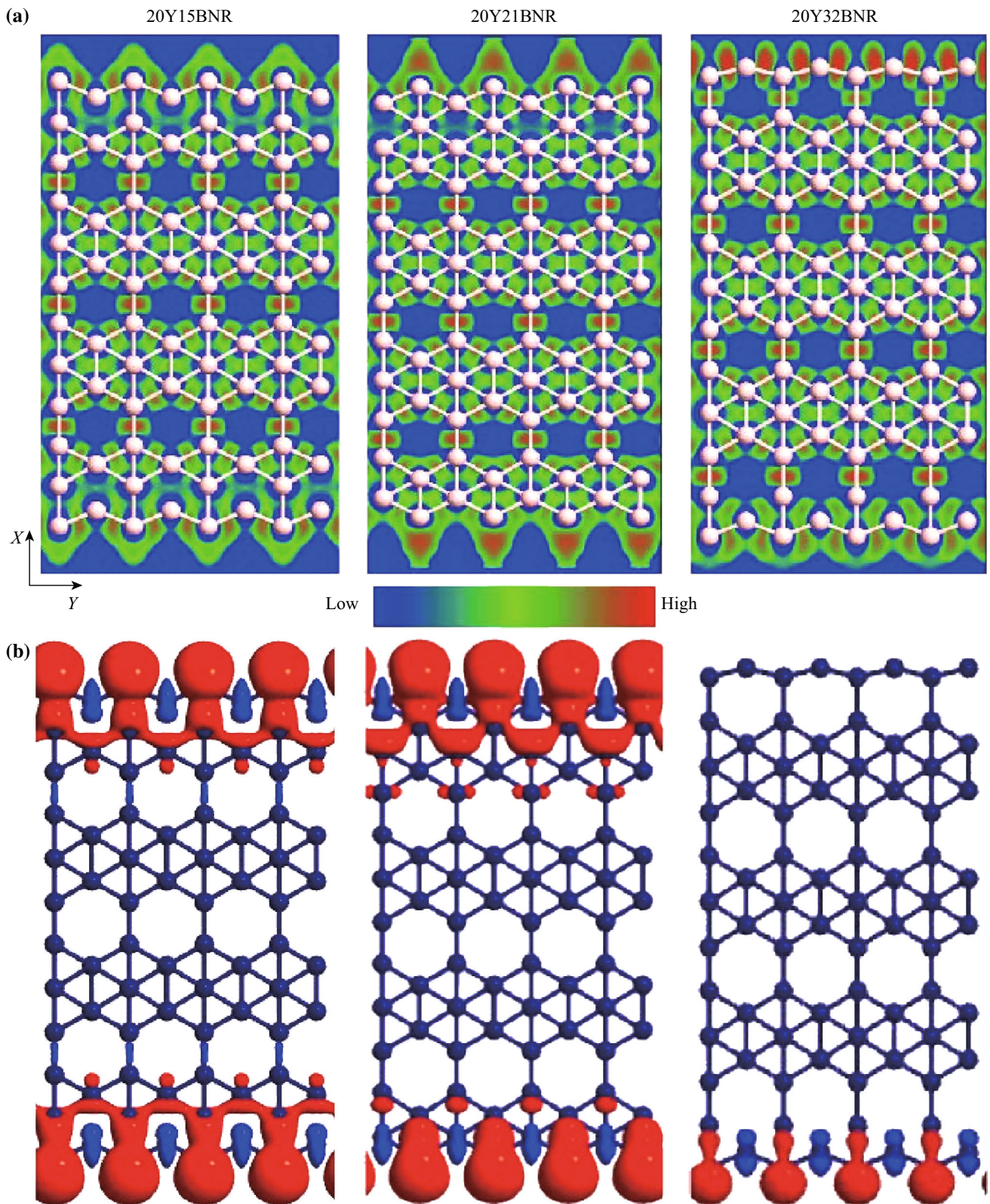
Fig. 8 **a** The electron localization function and **b** the spin density of *20YBNR* allotropes. The isovalue is 0.05
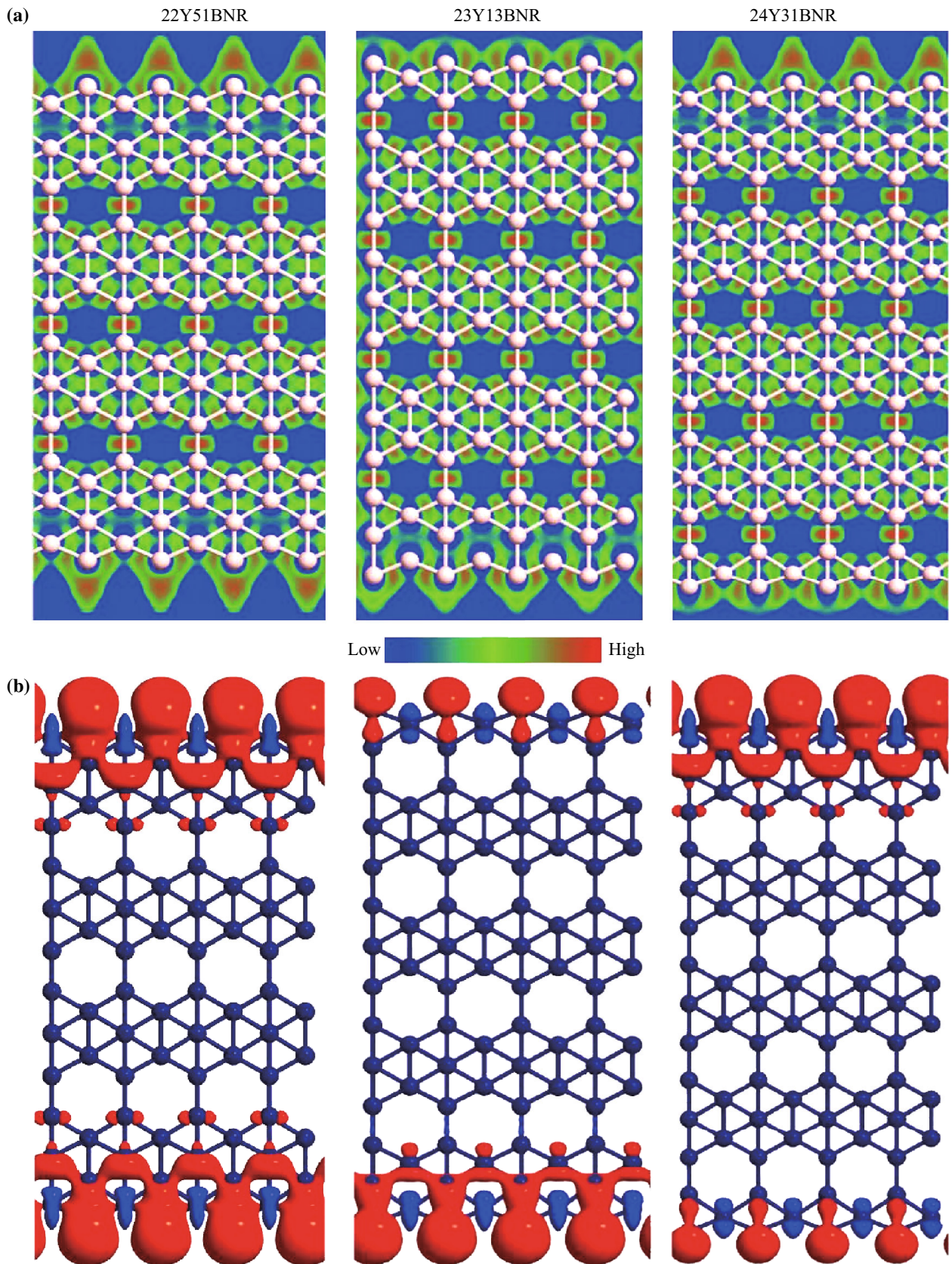
Fig. 9 **a** The electron localization function and **b** the spin density of *22Y51*, *23Y13*, and *24Y31*. The isovalue is 0.05
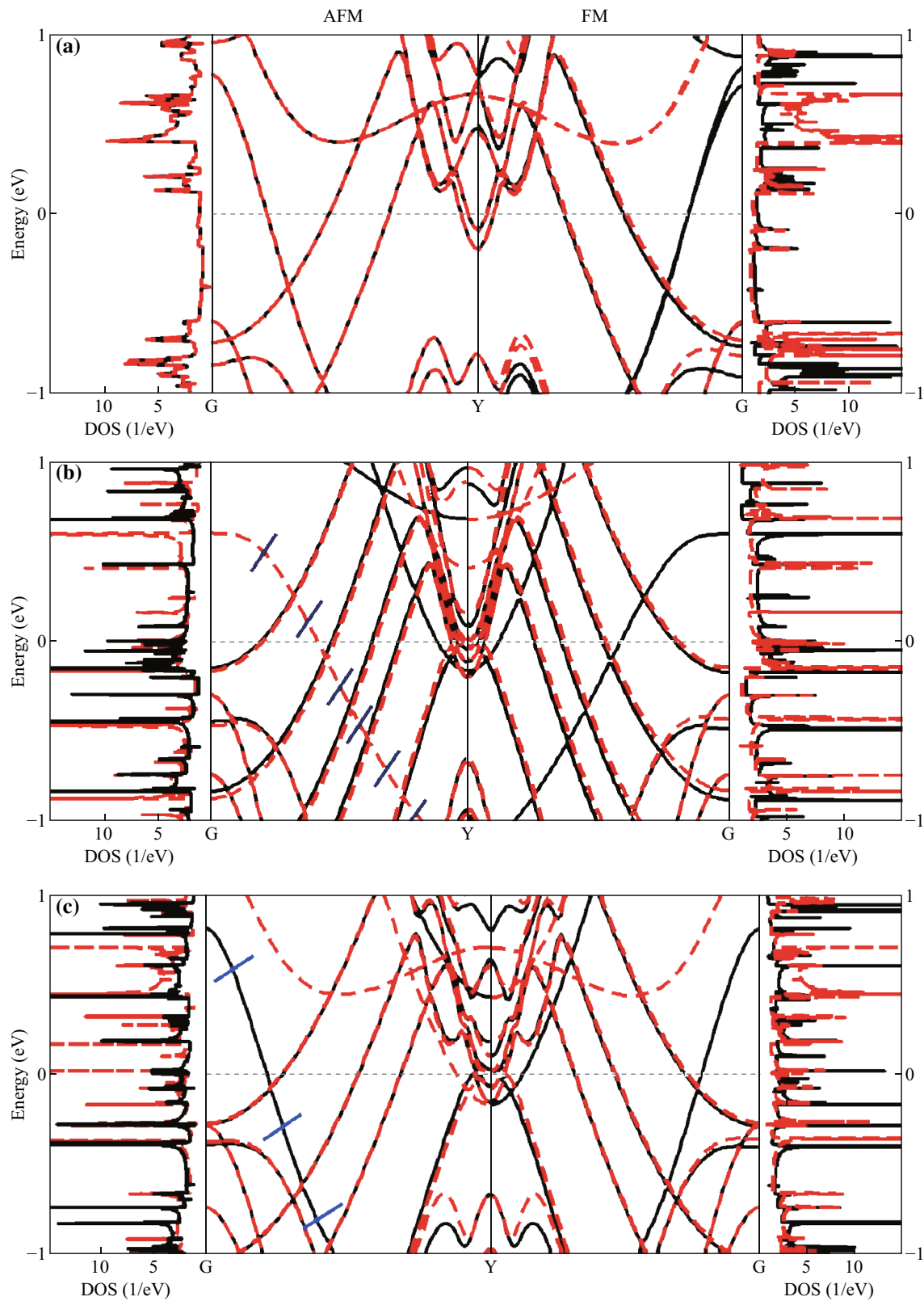
Fig. 10 Spin-dependent band structure of **a** *22Y51BNR*, **b** *23Y13BNR*, and **c** *24Y31BNR* in antiferromagnetic (AFM) and ferromagnetic (FM) configuration. The density of states of each configuration is also drawn. The oblique lines show bands which are arise due to the edge atom with highest magnetic moment. The dashed line is spin-down and the solid line is spin-up

Information. Figure 9a, b shows the ELF and spin density in the ferromagnetic configuration, respectively. The ELF shows why these ribbons are magnetic. The electron localization is observed in both edges. The energy difference between the magnetic and nonmagnetic states of 22Y51BNR is more than others because both the edges are composed of fully occupied hexagonal lattices. It is clear that the electron localization is weaker in hexagonal hole lattices like *23Y13BNR*. The edge atoms are coupled to their neighboring atoms antiferromagnetically in the *y*-direction and ferromagnetically in the *x*-direction. *22Y15* exhibits the strongest magnetization with a magnetic moment of 0.75 μ_B at both edges. The most spin anisotropy is observed in *24Y31* with a magnetic moment difference (between two edges) of 0.54 μ_B. Here, the upper edge has the higher magnetic moment. The spin anisotropy gives rise to spin splitting of the band structure in the antiferromagnetic configuration, as shown in Fig. 10. Although one expects that the band structure becomes spin degenerate in the antiferromagnetic configuration, the structural anisotropy of the edges breaks degeneracy and the bands become spin dependent.

The results show that cutting β_{12} sheet cannot induce a band gap in the structure. Therefore, all the ribbons are metals, which is in good agreement with the recent experimental results [41]. Figure 10 describes the band structure and the density of states (DOS) in the ferromagnetic and antiferromagnetic configurations. Each of the sharp peak of the DOS corresponds to an extremum of band structure or a flat band indicating strong electron localization. We found that the spin anisotropy significantly affects the band structure of the antiferromagnetic configuration so that there are bands that are dependent on the spin orientation of the edge atom with the highest magnetic moment. The bands are marked by a line in Fig. 10. We assumed that the spin orientation of the mentioned atom is spin-down in *23Y13*. Therefore, the bands are formed from the spin-down electrons. With regard to *24Y31*, the spin orientation is set to be spin-up for the atoms with the highest magnetic moment in the antiferromagnetic configuration. Note that these bands are a direct consequence of the spin anisotropy that was not reported in the previous studies pertaining to Borophene nanoribbons [15].

We did not consider the role of the substrate on the electronic and magnetic properties of the nanoribbons. We expect that the substrate reduces the anisotropy of the structure and moderates the conductance of the structure. However, it was shown that the β_{12} borophene is a metal, and it exhibits a Dirac cone in the presence of the supported Ag [6]. On the other hand, the recent experimental results showed that the synthesized ribbons are metals, and they are flat. Therefore, we expect that the spin anisotropy

reported in the article is a robust feature of some width of the ribbon, and it will exist in the presence of the substrate. Reference [46] shows that the charge transfer from the substrate to the BNR improves the electronic conductance of the ribbon. The spin anisotropy makes the β_{12} nanoribbons a potential candidate for future spintronic and spin filtering devices. Unlike previous nanoribbons like graphene nanoribbons, silicene nanoribbons, or germanene nanoribbons, β_{12}-BNRs have significant diversity in their individual characteristics, which make them an interesting candidate for the next-generation electronic devices.

4 Summary

We have analyzed freestanding β_{12}-BNRs using the density functional theory. The structural, electrical, and magnetic properties of the ribbons are studied in detail. It was found that the magnetization of ribbon is strongly dependent on its structural properties. The results show that all the ribbons considered here are metals, and some of them can be magnetic. Magnetization is solely observed in the ribbons prepared by cutting the borophene sheet along the *y*-direction *YBNR* and in some widths. Generally, *YBNRs* are more interesting in a sense that some ribbons can be magnetic at one or two edges in specific widths. In addition, spin anisotropy is observed in *YBNRs*, making one edge more magnetic than the other. The spin anisotropy arises from the asymmetry at the edge of the ribbon. The spin anisotropy makes the β_{12}-BNRs a potential candidate for spintronic applications.

References

1. A.J. Mannix, X.-F. Zhou, B. Kiraly, J.D. Wood, D. Alducin et al., Synthesis of borophenes: anisotropic, two-dimensional boron polymorphs. Science **350**(6267), 1513–1516 (2015). doi:10.1126/science.aad1080

2. B. Feng, J. Zhang, Q. Zhong, W. Li, S. Li et al., Experimental realization of two-dimensional boron sheets. Nat. Chem. **8**(6), 563–568 (2016). doi:10.1038/nchem.2491

3. X. Wu, J. Dai, Y. Zhao, Z. Zhuo, J. Yang, X.C. Zeng, Two-dimensional boron monolayer sheets. ACS Nano **6**(8), 7443–7453 (2012). doi:10.1021/nn302696v

4. Z. Zhang, A.J. Mannix, Z. Hu, B. Kiraly, N.P. Guisinger, M.C. Hersam, B.I. Yakobson, Substrate-induced nanoscale undulations

of borophene on silver. Nano Lett. **16**(10), 6622–6627 (2016). doi:10.1021/acs.nanolett.6b03349

5. B. Feng, J. Zhang, R.-Y. Liu, T. Iimori, C. Lian et al., Direct evidence of metallic bands in a monolayer boron sheet. Phys. Rev. B **94**(4), 041408 (2016). doi:10.1103/PhysRevB.94.041408

6. B. Feng, O. Sugino, R.-Y. Liu, J. Zhang, R. Yukawa, M. Kawamura, Dirac fermions in Borophene. Phys. Rev. Lett. **118**(9), 096401 (2017). doi:10.1103/PhysRevLett.118.096401

7. M. Ezawa, Triplet fermions and Dirac fermions in borophene. Phys. Rev. B **96**, 035425 (2017). doi:10.1103/PhysRevB.96.035425

8. A. Lopez-Bezanilla, P.B. Littlewood, Electronic properties of 8-Pmmn borophene. Phys. Rev. B **93**, 241405 (2016). doi:10.1103/PhysRevB.93.241405

9. A. Garcia-Fuente, J. Carrete, A. Vega, L.J. Gallego, How will freestanding borophene nanoribbons look like? An analysis of their possible structures, magnetism and transport properties. Phys. Chem. Chem. Phys. **19**(2), 1054–1061 (2017). doi:10.1039/C6CP07432D

10. A.D. Zabolotskiy, Y.E. Lozovik, Strain-induced pseudomagnetic field in the Dirac semimetal borophene. Phys. Rev. B **94**, 165403 (2016). doi:10.1103/PhysRevB.94.165403

11. A. Lherbier, A.R. Botello-Méndez, J.-C. Charlier, Electronic and optical properties of pristine and oxidized borophene. 2D Mater. **3**, 045006 (2016). doi:10.1088/2053-1583/3/4/045006/meta

12. B. Peng, H. Zhang, H. Shao, Y. Xu, R. Zhang, H. Zhu, The electronic, optical, and thermodynamic properties of borophene from first-principles calculations. Mater. Chem. C **4**(16), 3592–3598 (2016). doi:10.1039/C6TC00115G

13. J. Carrete, W. Li, L. Lindsay, D.A. Broido, L.J. Gallego, N. Mingoa, Physically founded phonon dispersions of few-layer materials and the case of borophene. Mater. Res. Lett. **4**(4), 204–211 (2016). doi:10.1080/21663831.2016.1174163

14. F. Ma, Y. Jiao, G. Gao, Y.T. Gu, A. Bilic, Z. Chen, A. Du, Graphene-like two dimensional ionic boron with double Dirac cones at ambient condition. Nano Lett. **16**(5), 3022–3028 (2016). doi:10.1021/acs.nanolett.5b05292

15. H. Shu, F. Li, P. Liang, X. Chen, Unveiling the atomic structure and electronic properties in atomically thin boron sheets on Ag(111) surface. Nanoscale **8**(36), 16284–16291 (2016). doi:10.1039/C6NR02871C

16. M.Q. Le, B. Mortazavi, T. Rabczuk, Mechanical properties of borophene films: a reactive molecular dynamics investigation. Nanotechnology **27**(44), 445709 (2016). doi:10.1088/0957-4484/27/44/445709

17. T. Tsafack, B.I. Yakobson, Thermomechanical analysis of two-dimensional boron monolayers. Phys. Rev. B **93**(16), 165434 (2016). doi:10.1103/PhysRevB.93.165434

18. V. Wang, W.T. Geng, Lattice defects and the mechanical anisotropy of borophene. J. Phys. Chem. C **121**(18), 10224–10232 (2017). doi:10.1021/acs.jpcc.7b02582

19. H. Wang, Q. Li, Y. Gao, F. Miao, X.-F. Zhou, X.G. Wan, Strain effects on borophene: ideal strength, negative Possion's ratio and phonon instability. New J. Phys. **18**(7), 073016 (2016). doi:10.1088/1367-2630/18/7/073016

20. G.I. Giannopoulos, Mechanical behavior of planar borophenes: a molecular mechanics study. Comput. Mater. Sci. **129**, 304–310 (2017). doi:10.1016/j.commatsci.2016.12.045

21. J. Yuan, N. Yu, K. Xue, X. Miao, Ideal strength and elastic instability in single-layer 8-Pmmn borophene. RSC Adv. **7**(14), 8654–8660 (2017). doi:10.1039/C6RA28454J

22. Z. Zhang, Y. Yang, E.S. Penev, B.I. Yakobson, Elasticity, flexibility, and ideal strength of borophenes. Adv. Funct. Mater. **27**(9), 1605059 (2017). doi:10.1002/adfm.201605059

23. M. Gao, Q.-Z. Li, X.-W. Yan, J. Wang, Prediction of phonon-mediated superconductivity in borophene. Phys. Rev. B **95**(2), 024505 (2017). doi:10.1103/PhysRevB.95.024505

24. R.C. Xiao, D.F. Shao, W.J. Lu, H.Y. Lv, J.Y. Li, Y.P. Sun, Enhanced superconductivity by strain and carrier-doping in borophene: a first principles prediction. Appl. Phys. Lett. **109**(12), 122604 (2016). doi:10.1063/1.4963179

25. Y. Zhao, S. Zeng, J. Ni, Phonon-mediated superconductivity in borophenes. App. Phys. Lett. **108**(24), 242601 (2016). doi:10.1063/1.4953775

26. Y. Zhao, S. Zeng, J. Ni, Superconductivity in two-dimensional boron allotropes. Phys. Rev. B **93**(1), 014502 (2016). doi:10.1103/PhysRevB.93.014502

27. C. Cheng, J.-T. Sun, H. Liu, H.-X. Fu, J. Zhang, X.-R. Chen, S. Meng, Suppressed superconductivity in substrate-supported β12 borophene by tensile strain and electron doping. 2D Mater. **4**(2), 025032 (2017). doi:10.1088/2053-1583/aa5e1b/meta

28. G. Liu, H. Wang, Y. Gao, J. Zhou, H. Wang, Anisotropic intrinsic lattice thermal conductivity of borophene from first-principles calculations. Phys. Chem. Chem. Phys. **19**(4), 2843–2849 (2017). doi:10.1039/C6CP07367K

29. J.C. Alvarez-Quiceno, R.H. Miwa, G.M. Dalpian, A. Fazzio, Oxidation of free-standing and supported borophene. 2D Mater. **4**(2), 025025 (2017). doi:10.1088/2053-1583/aa55b6/meta

30. Y. Jiao, F. Ma, J. Bell, A. Bilic, A. Du, Two-dimensional boron hydride sheets: high stability, massless Dirac fermions, and excellent mechanical properties. Angew. Chem. Int. Ed. **55**(35), 10292–10295 (2016). doi:10.1002/ange.201604369

31. Z.-Q. Wang, T.-Y. Lu, H.-Q. Wang, Y.-P. Feng, J.-C. Zheng, High anisotropy of fully hydrogenated borophene. Phys. Chem. Chem. Phys. **18**(46), 31424–31430 (2016). doi:10.1039/C6CP06164H

32. Z.-Q. Wang, T.-Y. Lu, H.-Q. Wang, Y.P. Feng, J.-C. Zheng, New crystal structure prediction of fully hydrogenated borophene by first principles calculations. Sci. Rep. **7**(1), 609 (2017). doi:10.1038/s41598-017-00667-x

33. H.R. Jiang, Z. Lu, M.C. Wu, F. Ciucci, T.S. Zhao, Borophene: a promising anode material offering high specific capacity and high rate capability for lithium-ion batteries. Nano Energy **23**, 97–104 (2016). doi:10.1016/j.nanoen.2016.03.013

34. B. Mortazavi, A. Dianat, O. Rahaman, G. Cuniberti, T. Rabczuk, Borophene as an anode material for Ca, Mg, Na or Li ion storage: a first-principle study. J. Power Sour. **329**, 456–461 (2016). doi:10.1016/j.jpowsour.2016.08.109

35. B. Mortazavi, O. Rahaman, S. Ahzi, T. Rabczukc, Flat borophene films as anode materials for Mg, Na or Li-ion batteries with ultrahigh capacities: a first-principles study. Appl. Mater. Today **8**, 60–67 (2017). doi:10.1016/j.apmt.2017.04.010

36. J.E. Padilha, R.H. Miwa, A. Fazzio, Directional dependence of the electronic and transport properties of 2D borophene and borophane. Phys. Chem. Chem. Phys. **18**(36), 25491–25496 (2016). doi:10.1039/C6CP05092A

37. S. Izadi Vishkayi, M. Bagheri Tagani, Current-voltage characteristics of borophene and borophane sheets. Phys. Chem. Chem. Phys. **19**(32), 21461–21466 (2017). doi:10.1039/C7CP03873A

38. Y.-W. Son, M.L. Cohen, S.G. Louie, Half-metallic graphene nanoribbons. Nature **444**(7117), 347–349 (2006). doi:10.1038/nature05180

39. X. Li, X. Wang, L. Zhang, S. Lee, H. Dai, Chemically derived, ultrasmooth graphene nanoribbon semiconductors. Science **319**(5867), 1229–1232 (2008). doi:10.1126/science.1150878

40. F. Meng, X. Chen, S. Sun, J. He, Electronic and magnetic properties of pristine and hydrogenated borophene nanoribbons. Physica E **91**, 106–112 (2017). doi:10.1016/j.physe.2017.04.014

41. Q. Zhong, L. Kong, J. Gou, W. Li, S. Sheng et al., Synthesis of borophene nanoribbons on Ag(110) surface. Phys. Rev. Mater. **1**, 021001(R) (2017). doi:10.1103/PhysRevMaterials.1.021001

42. Q. Zhong, J. Zhang, P. Cheng, B. Feng, W. Li et al., Metastable phases of 2D boron sheets on Ag(111). J. Phys. Condens. Matter **29**(9), 095002 (2017). doi:10.1088/1361-648X/aa5165

43. E. Artacho, D. Sanchez-Portal, P. Ordejon, A. Garcia, J.M. Soler, Density functional method for very large systems with LCAO basis sets. Int. J. Quantum Chem. **65**(5), 453–461 (1997). doi:10.1002/(SICI)1097-461X(1997)65:5<453:AID-QUA9>3.0.CO;2-V

44. N. Troullier, J.L. Martins, Efficient pseudopotentials for plane-wave calculations. Phys. Rev. B **43**(3), 1993–2006 (1991). doi:10.1103/PhysRevB.43.1993

45. J.P. Perdew, K. Burke, M. Ernzerhof, Generalized gradient approximation made simple. Phys. Rev. Lett. **77**(18), 3865 (1996). doi:10.1103/PhysRevLett.77.3865

46. Y. Liu, Y.-J. Dong, Z. Tang, X.-F. Wang, L. Wang, T. Hou, H. Lin, Y. Li, Stable and metallic borophene nanoribbons from first-principles calculations. J. Mater. Chem. C **4**(26), 6380 (2016). doi:10.1039/C6TC01328G